CHAPTER IV
RESULTS AND DISCUSSION

In this chapter, the catalysts were characterized using many methods, and the results are shown in Sections 4.1 to 4.4. Moreover, the activities of catalysts were tested for the dehydration of bio-ethanol. The set of catalysts and abbreviations are shown in Table 4.1.

Table 4.1 Catalysts and abbreviation in experiments

1st scope		
# of run	**Catalysts (Si/Al_2)**	**Abbreviation**
1	H-Beta (27)	B27
2	H-Beta (37)	B37
3	H-Beta (300)	B300
4	5wt%GeO_2/H-Beta (27)	5Ge'B27
5	5wt%GeO_2/H-Beta(37)	5Ge'B37
6	5wt%GeO_2/H-Beta (300)	5Ge'B300
7	5wt%Ga_2O_3/H-Beta (27)	5Ga'B27
8	5wt%Ga_2O_3/H-Beta (37)	5Ga'B37
9	5wt%Ga_2O_3/H-Beta (300)	5Ga'B300
2nd scope		
10	MSU-S/H_{BEA}	MSU
11	5wt%GeO_2/ MSU-S/H_{BEA}	5Ge'MSU
12	5wt%Ga_2O_3/ MSU-S/H_{BEA}	5Ga'MSU

4.1 Effect of Acid Density and Acid Strength of H-Beta Zeolites

4.1.1 Characterization of Catalysts

X-ray Diffraction (XRD), Surface Area Analyzer (SAA), Temperature Programmed Desorption of Ammonia (TPD-NH_3), and Temperature Programmed

Desorption of Isopropylamine (TPD-IPA) were used to identify the specific characteristics of zeolites and the physical properties of catalysts as discussed in details later.

The XRD results are shown in Figure 4.1. The specific peaks of H-Beta zeolite consist of 2 theta at 7.6°, 14.6°, and 22.4° (Omegna *et al.*, 2004).

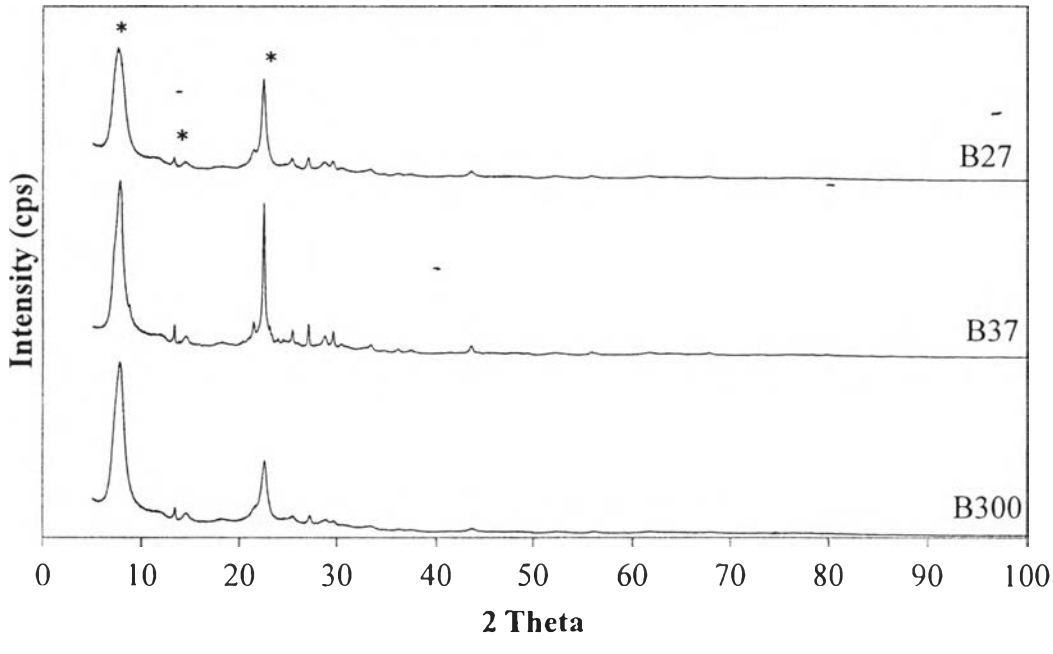

Figure 4.1 X-ray diffraction patterns of H-Beta catalysts.

The physical properties of catalysts are presented in Table 4.2. Surface area, pore volume, and pore diameter were determined by the Braunaer-Emmet-Teller (BET) and Horvath Kawazoe (HK) technique. The increasing Si/Al_2 ratio extremely reduces the surface area and pore volume of zeolites. B27, B37, and B300 have surface area 554.9 m^2/g, 502.7 m^2/g, and 425.9 m^2/g respectively, and they have pore volume 0.27 cm^2/g, 0.26 cm^2/g, and 0.20 cm^2/g respectively. However, the pore diameter of all catalysts in the experiment did not show clearly tendency but had value in the range of 7.68 Å to 8.67 Å.

Figure 4.2 shows the TPD-NH_3 results obtained from the zeolites with various ratios of Si/Al_2. The area of each peak represents the amount of acid sites. It can be observed that the area under curves and then the total acidity decrease with

the increasing Si/Al_2 ratio. Furthermore, the NH_3 desorption temperature also indicates the acid strength of zeolites; therefore, B27 has the highest acid strength, followed by B37 and then B300. From Figure 4.3, propylene desorption from TPD-IPA testing displays the acid density and acid strength in the same trends as observed from TPD-NH_3. In addition, the desorption of NH_3 (m/z = 17), C_3H_6 (m/z = 41), and C_3H_7-NH_2(m/z = 44) from the TPD-IPA experiment can distinguish between lewis acid and bronsted acid in zeolites. The IPA was pulsed in the reactor and adsorb on acid sites, but only bronsted acid sites are strong enough to break IPA molecules to ammonia and propylene, which subsequently desorb as probes indicating Bronsted acid sites. From Figures 4.3 and 4.4, ammonia or propylene peak, which exhibits around 300 °C to 500 °C, represents strong bronsted acid sites. Bronsted acid sites and Lewis acid sites are indicated by IPA desorption. The density of bronsted acid sites was calculated from propylene area. The strong bronsted acid density of B27, B37, and B300 are 2,367, 698.8, and 112.9 μmol/g catalysts, respectively. Strong bronsted acid density is ranked as follows; B27 > B37 > B300, and acid strength is ranked as follows; B27 > B37 > B300. B27 does not only have the highest strong bronsted acid density, but also have the highest weak acid density as shown in Figure 4.4. So, B27 has the highest acid density that is active for many reactions.

Table 4.2 Physical properties of catalysts

Catalysts	Si/Al_2 [a]	Surface Area (m^2/g) [b]	Pore Volume (cm^3/g) [c]	Pore Diameter (Å) [c]
B 27	27.20	554.9	0.27	7.68
B 37	33.06	502.7	0.26	7.93
B 300	350.7	425.9	0.20	8.67

[a] Determined by XRF technique
[b] Determined by BET method
[c] Determined by H.K. method

4.1.2 Activity on Catalytic Dehydration of Bio-ethanol

3 g of catalyst was packed into the U-tube reactor, and bio-ethanol was fed at 450°C. 97 % ethanol conversion was achieved over all Si/Al_2 ratio of H-Beta. Ethylene is produced from ethanol dehydration, and then ethylene is converted

into various hydrocarbon products, which is governed by various Si/Al_2 of H-Beta zeolite.

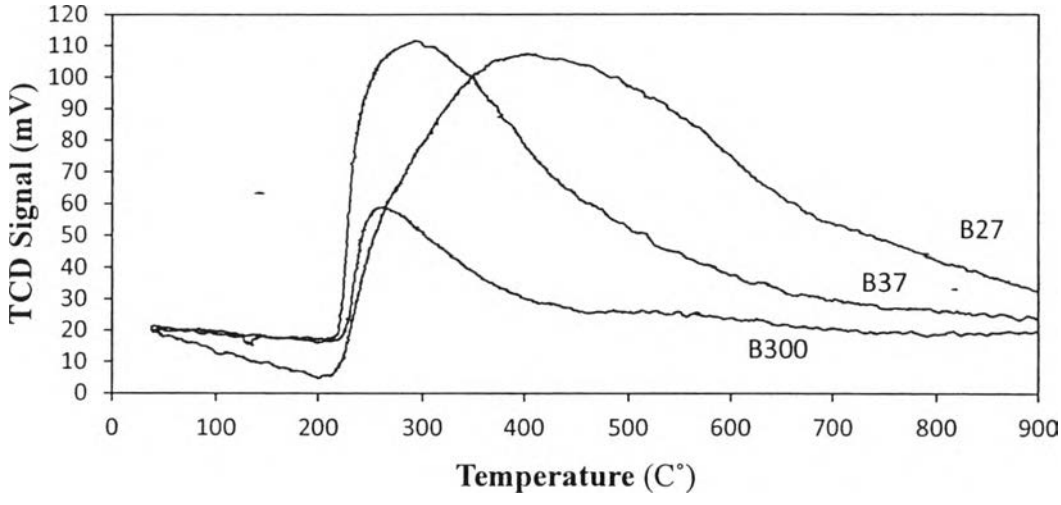

Figure 4.2 TPD-NH_3 of unloaded H-Beta zeolites with different Si/Al_2 ratio.

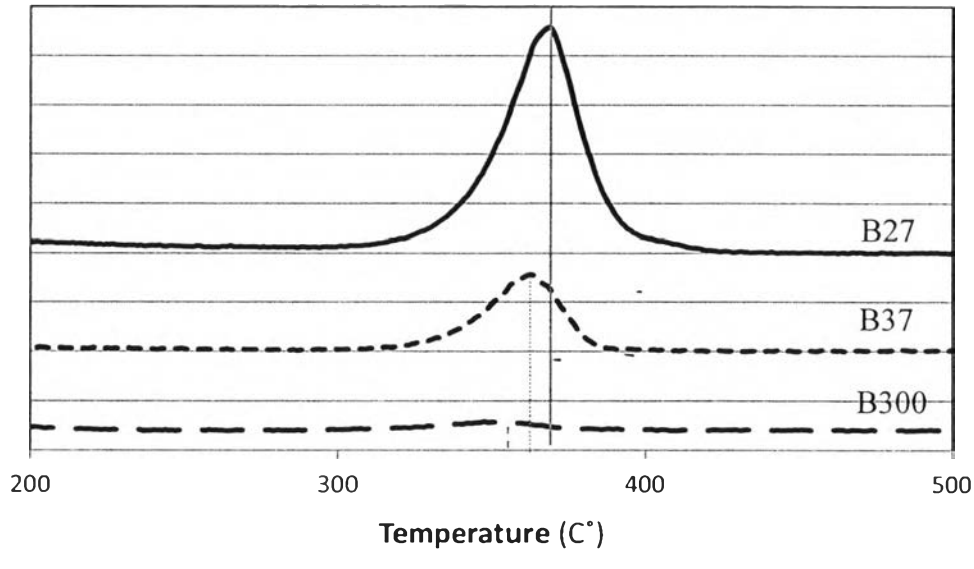

Figure 4.3 Propylene desorption profile of unloaded H-Beta zeolite with different Si/Al_2 ratio from TPD-IPA.

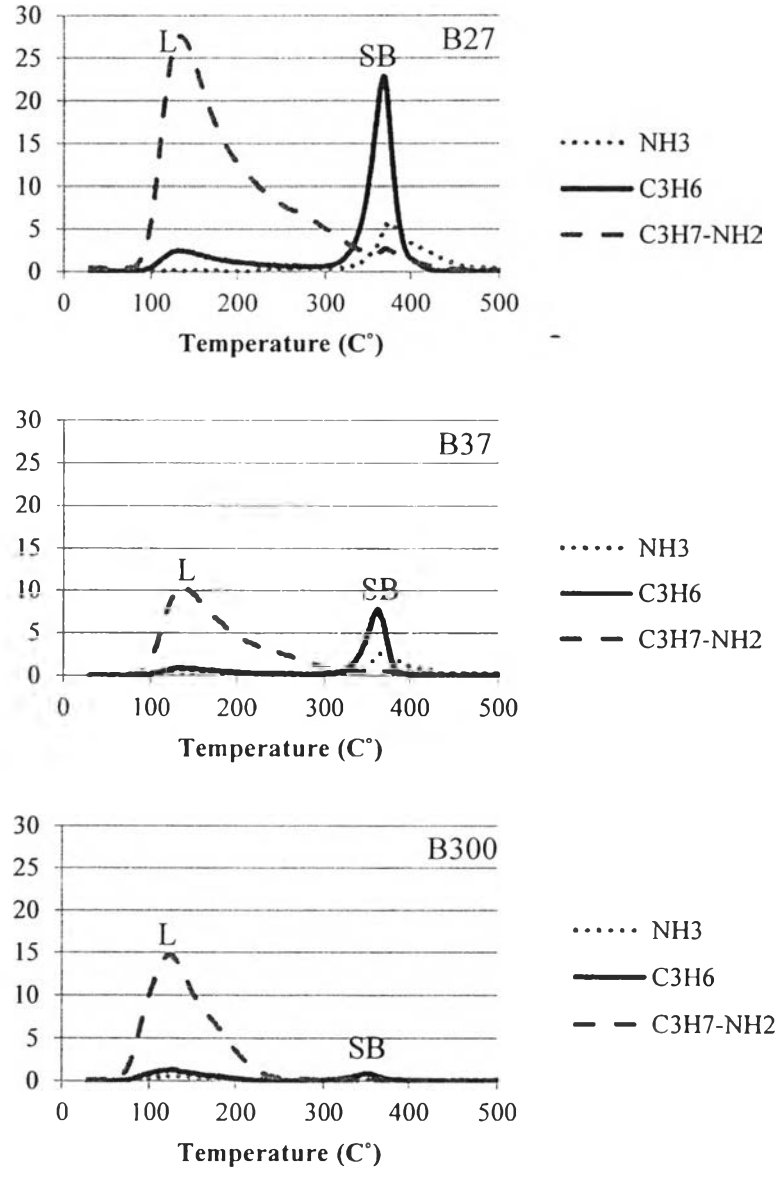

Figure 4.4 TPD-IPA profiles of unloaded H-Beta zeolite with different Si/Al_2 ratios.

Table 4.3 Strong Bronsted Acid amount over different Si/Al_2 ratios zeolites.

	B27	**B37**	**B300**
Strong Bronsted Acid (μmol/g of catalyst)	2,367.5	698.8	112.9

From Table 4.4, 75.8 % gas is produced using B27. The major gaseous component is ethylene, which is 85.9 % in the gas product. Ethylene is first

produced from ethanol dehydration, and then ethylene is converted into various hydrocarbon products, which is governed by acidity or Si/Al_2 of H-Beta zeolite. Nevertheless, 5.05% of oil is attained from secondary reactions in the reaction path way previously shown in Figure 2.5. As shown in Figure 4.6, the oil consists of 82.4 % BTEX, 14.4 % C_9 aromatics and a little amount of other hydrocarbons products. Moreover, among mixed xylene, B27 selectively produces only *p*-xylene, which exists 44.2 % in the oil product. Ethylene, which is the major component in the gaseous phase, can be further converted to benzene via oligomerization and aromatization reactions. After that, the alkylation of benzene with ethylene generates ethylbenzene, C_9 aromatics, and C_{10+} aromatics, as exhibited in Figure 4.6. A large amount of benzene, C_9 aromatics, and C_{10+} aromatics over a large number of acid sites on B 27 leads to dispropotionation and transalkylation reactions, as shown in Figure 4.8. Those reactions can give the large amount of *p*-xylene as shown in Figure 4.6.

In case of B37, the results show that only 63.0 % gas yield is achieved; hence, it decreases and contains a lower ethylene content than what observed from B 27. Table 4.4 shows that the oil yield is enhanced to 7.27 % higher than that of the other two zeolites because of the moderate acidity of B 37. Hence, only about 80 % ethylene is produced from B 37 because some ethylene might be converted to larger hydrocarbons in the oil range, resulted in the lowest gas yield. The oil content from B 37 mainly consists of 40 % BTEX (mainly composed of 26.7 % mixed xylenes), 38.8 % C_9 aromatics, and 24.8 % C_{10}^+ aromatics. For this Si/Al_2 ratio, C_9- and C_{10}^+ aromatics are produced in very large amounts when compared with those from the other Si/Al_2 ratios. The results show the decreases of ethylene and benzene, but C_9- and C_{10}^+ aromatics are enhanced. A large of C_9- and C_{10}^+ aromatics may be formed by alkylation reaction as shown in Figure 4.9. Nevertheless, the moderate acidity of B 37 suppresses disproportionation and transalkylation reactions. So, toluene and xylenes are produced in a low amount, but C_9- and C_{10}^+ aromatics still are present plenty. B 37, which have moderate acidity, has a tendency to convert bio-ethanol into heavy hydrocarbons. Therefore, B 37 should be a good catalyst for producing heavy hydrocarbons.

Using B 300, as high as around 81.5 % gas in the product, is achieved. The major component of gaseous compounds is ethylene existing in a very high content of around 94.6 % in gas. Thus, 5.43 % oil yield is obtained as shown in Table 4.4. The oil components obtained from B 300 are comprised of oxygenate compounds (4.08 %), non-aromatic compounds (17.2 %), benzene (36.2 %), xylenes (25.5 %), ethylbenzene (2.05 %), C_9 aromatics (12.3 %), and C_{10}^+ aromatics (2.72 %). It can be noticed that oxygenate compounds, non-aromatics and benzene are enhanced over the low acid density of B 300. Some of ethylene may convert to non-aromatics and benzene. However, scant acid density is not enough for alkylation, dispropotionation and transalkylation reaction, resulting in a little quantity of xylenes, ethylbenzene, C_9 aromatics, and C_{10}^+ aromatics.

Therefore, the moderate acid density and acid strength of B37 tends to convert ethylene to larger hydrocarbons; whereas the lower acid density of B300 produces ethylene mostly.

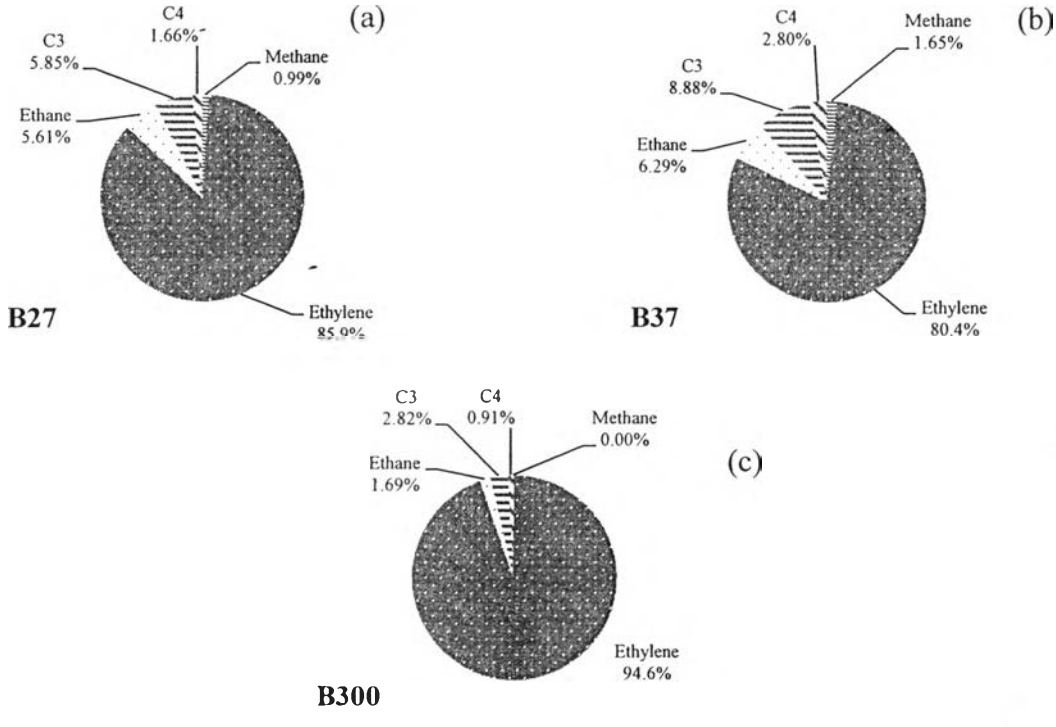

Figure 4.5 Composition of gases from (a) B 27, (b) B 37, and (c) B 300.

Table 4.4 Product distribution over B27, B37, and B300

Catalyst	B27	B37	B300
Bio-ethanol Conversion (%)	97.4	97.4	97.4
Product Distribution (wt %)			
Gas	75.8	63.0	81.5
Oil	5.05	7.27	5.43
Water	19.2	29.7	13.1
Gas Composition (wt %)			
Methane	0.99	1.65	0.00
Ethylene	85.9	80.4	94.6
Ethane	5.61	6.29	1.69
C3	5.85	8.88	2.82
C4	1.66	2.80	0.91
CO_2	0.00	0.00	0.00

Data were taken at the eighth hour of time-on-stream

Xylenes are valuable petrochemicals that have high costs. Both Si/Al_2 ratios of H-beta catalysts (B27 and B300) prefer to produce *p*-xylene around a half of overall xylenes selectivity, except B37 that mainly produces *m*-xylene as shown in Figure 4.7. Table 4.5 shows that B27 can provide the highest amount *p*-xylene in oil and the large amount *p*-xylene in mixed xylenes because disproportionations of large hydrocarbons occur from a high acid density of B27.

4.2 Effect of Gallium Oxides Loaded on Beta Zeolites

This part focuses on the effect of metal oxides loaded on Beta zeolites. The product distribution can be changed when the modified zeolites are used. 5 % of gallium oxide was loaded into the zeolites using the incipient wetness impregnation technique.

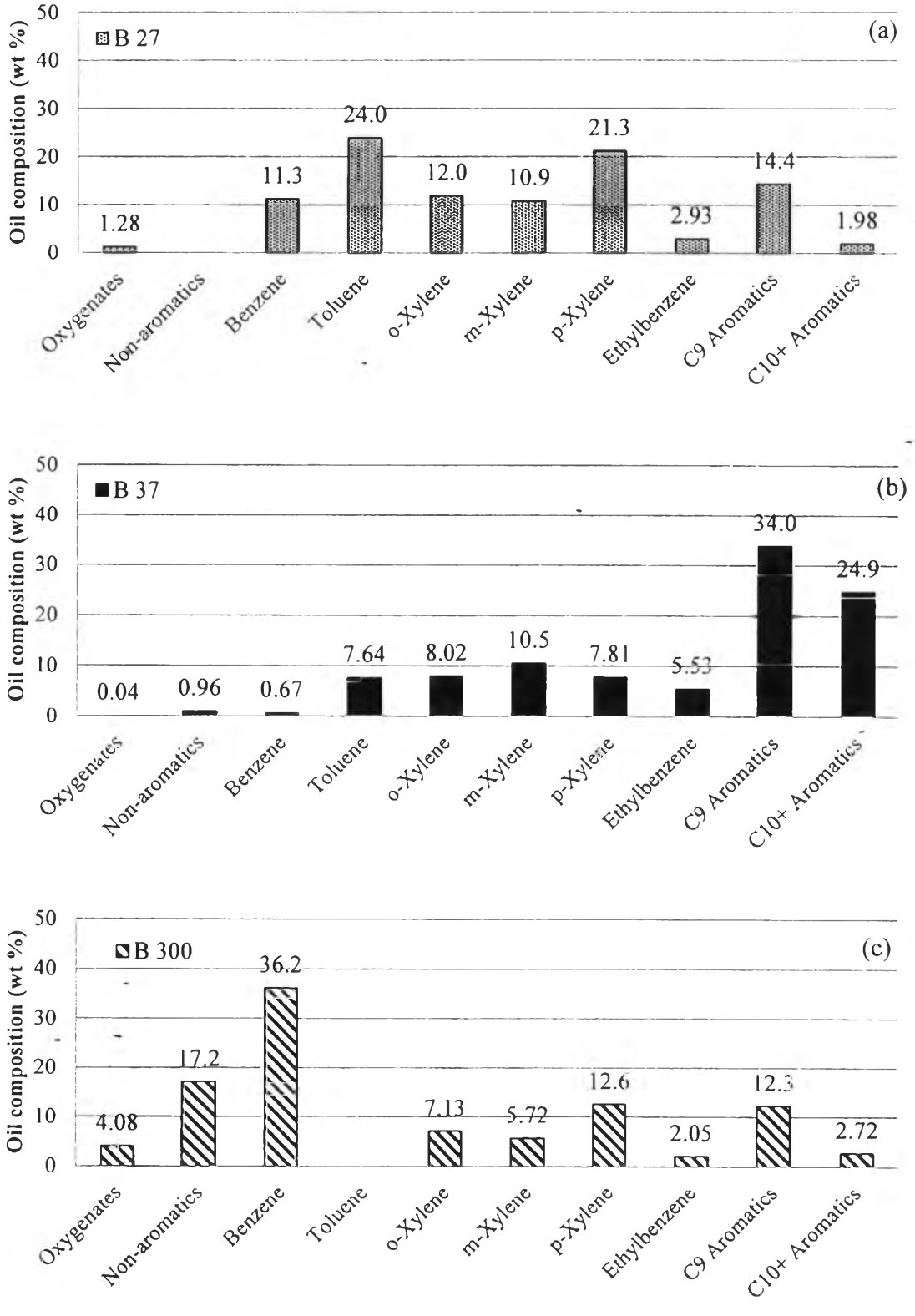

Figure 4.6 Composition of extracted oils from (a) B 27, (b) B 37, and (c) B 300.

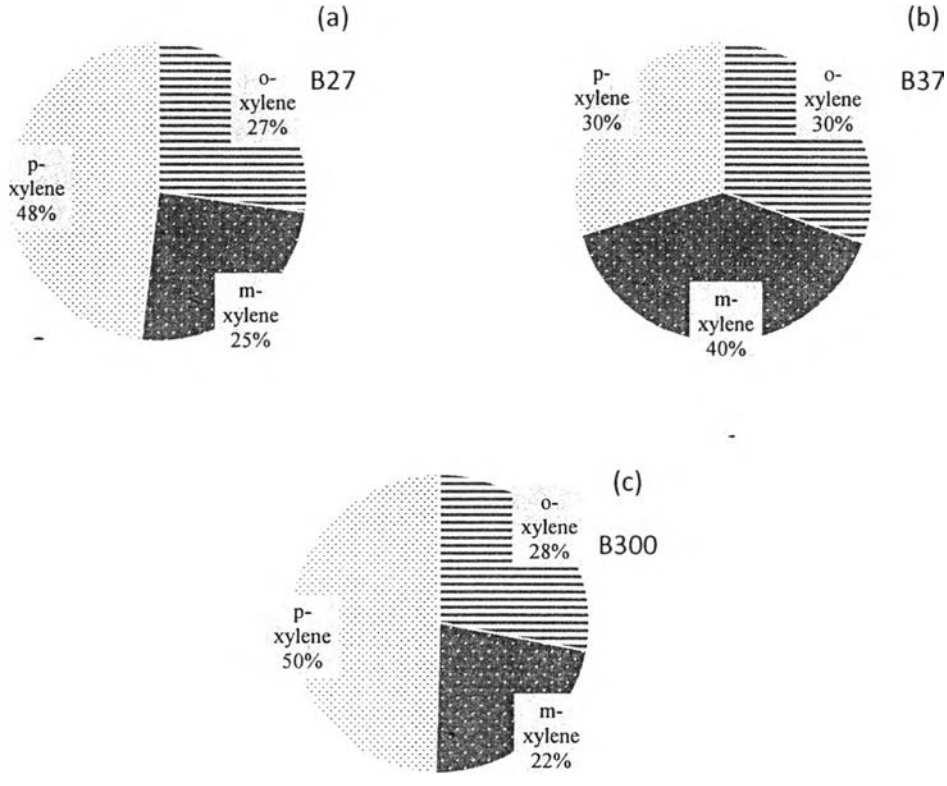

Figure 4.7 Selectivity of xylene isomers from (a) B27, (b) B37, and (c) B300

Table 4.5 *p*-Xylene amount in different components

Catalyst	B27	B37	B300
Mixed Xylenes (wt %)	44.2	26.4	25.5
p-Xylene in Oil (wt %)	21.3	7.81	12.6
p-Xylene in Mixed Xylenes (wt %)	48.2	29.6	49.6
p-Xylene in Mixed Aromatics (wt %)	21.6	7.89	16.1

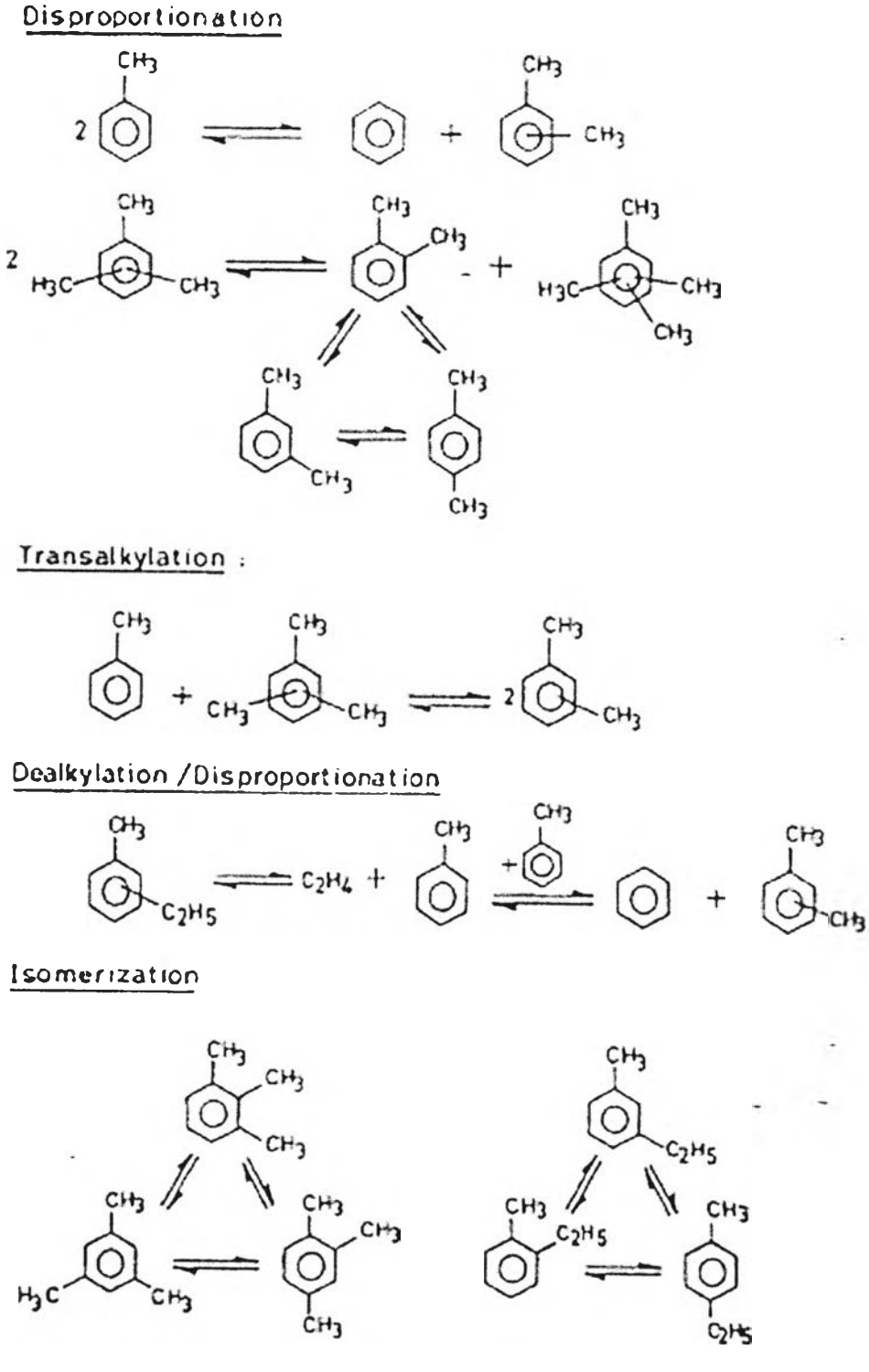

Figure 4.8 Reaction pathways of aromatic compounds (Das *et al.*, 1994).

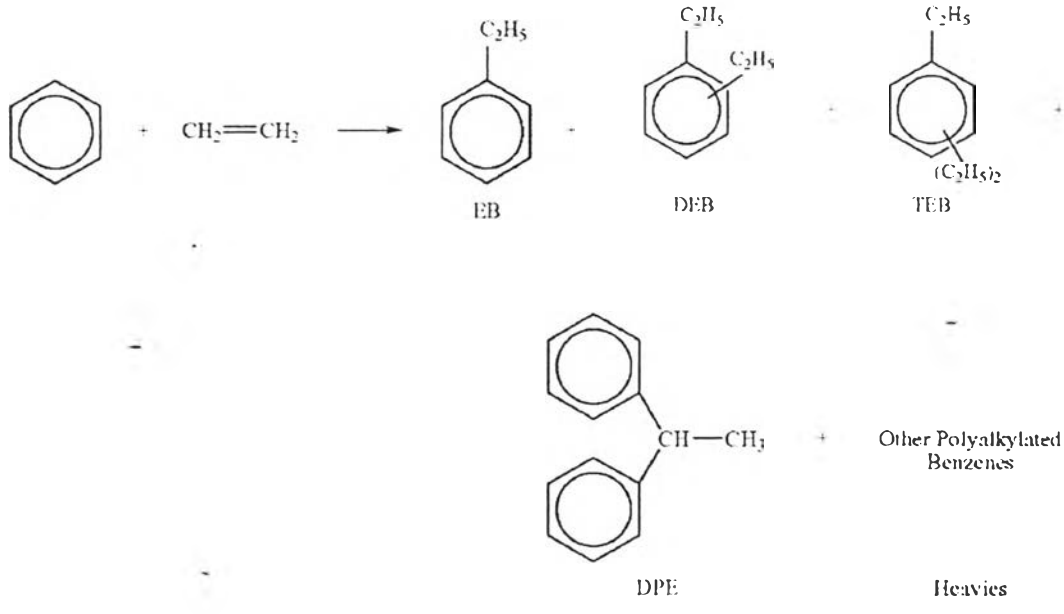

Figure 4.9 Alkylation reaction of benzene with ethylene (Jan *et al.*, 2007).

4.2.1 Characterization of Catalysts

The specific peaks of H-Beta zeolites, shown in Figure 4.10 (a), are located at the 2 theta of 7.6°, 14.6°, and 22.4° (Omegna *et al.*, 2004). Moreover, Figure 4.11 shows the gallium oxide's characteristic peaks at 52.3 °, 56.1 °, 61.9 °, and 68.1°. However, the specific peaks of H-Beta zeolite are still present in the XRD patterns after loading with gallium oxides, meaning that the metal oxide loading does not destroy the zeolite structures.

The physical properties of catalysts are presented in Table 4.6. Surface area, pore volume, and pore diameter were determined using the Braunaer-Emmet-Teller (BET) and Horvath Kawazoe (H.K.) techniques. Gallium oxide loading reduces the surface area and pore volume of unloaded zeolites because of pore blocking by the oxide as shown in Table 4.6. Moreover, the increasing Si/Al_2 ratio extremely reduces the surface area and pore volume of zeolites. 5GaB27, 5GaB37, and 5GaB300 have the surface area of 495.7 m^2/g, 354.0 m^2/g, and 236.8 m^2/g, respectively, and the pore volume reduces with the same trend.

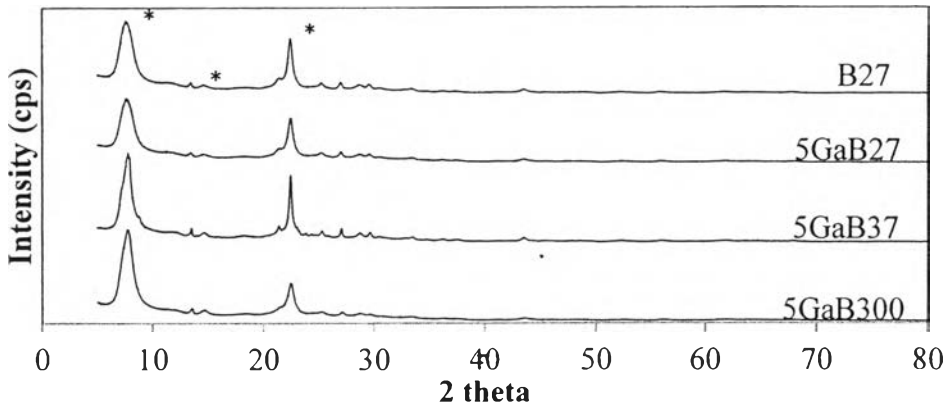

Figure 4.10 XRD characteristic peaks of H-Beta.

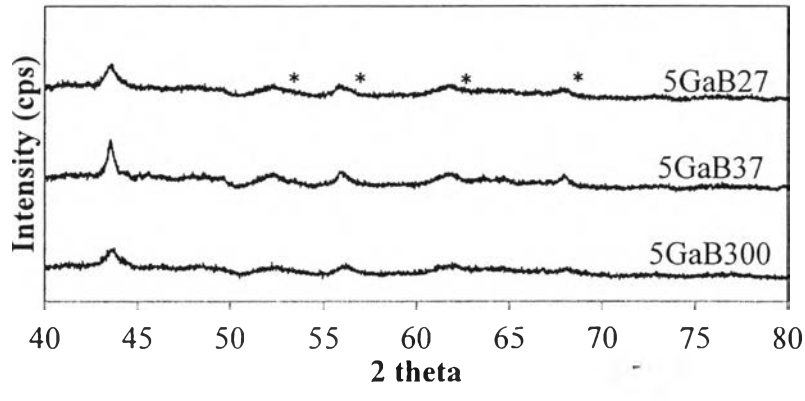

Figure 4.11 XRD characteristic peaks of gallium oxide loaded H-Beta catalysts.

The acidity of modified zeolites with various ratios of Si/Al_2 was analysed using TPD-NH_3. The area under each peak represents the amount of acid sites as shown in Figure 4.12. Total acidity is ranked as follows: 5GaB37 > 5GaB27 > 5GaB300. Moreover, the NH_3 desorption temperature also indicates the acid strength of zeolites; that is, 5GaB27 has the highest acid strength, followed by 5GaB37 and then 5GaB300. Figure 4.13 displays Lewis and Bronsted acid sites of zeolite after gallium oxide loading. The acid density and acid strength intensely decrease with gallium oxide loading as shown in Figures 4.13 and 4.14, and Table 4.7.

Table 4.6 Physical properties of H-Beta supports and 5 wt % gallium oxide loadved H-Beta catalysts

Catalysts	B27	5GaB27	B37	5GaB37	B300	5GaB300
Surface Area[a] (m^2/g)	554.9	495.7	502.7	354.0	425.9	236.8
Pore Volume[b] (cm^2/g)	0.27	0.24	0.26	0.18	0.20	0.13
Pore Diameter[b] (Å)	7.68	7.75	7.93	8.02	8.67	7.52

[a] Determined by BET method
[b] Determined by H.K. method

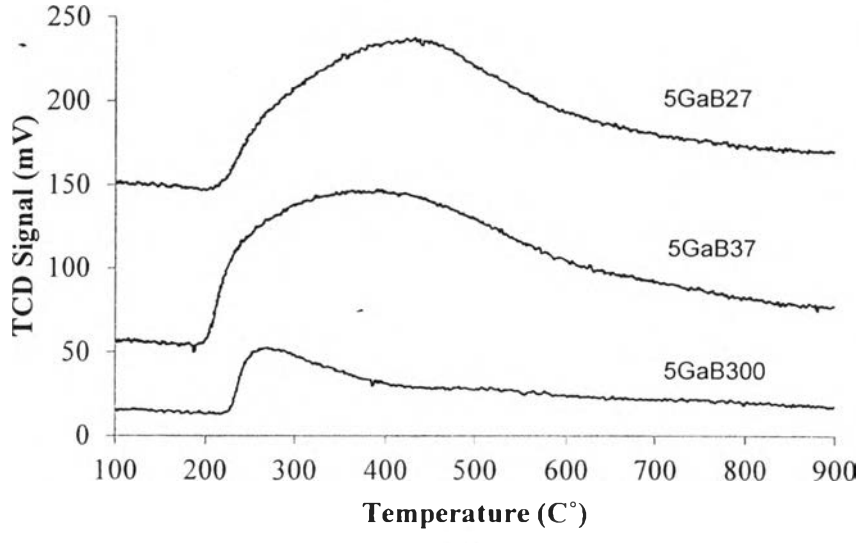

Figure 4.12 TPD-NH_3 profile of 5% wt gallium oxide loaded H-Beta catalysts.

Table 4.7 Density of Bronsted acid sites over unloaded H-Beta and 5 wt % gallium oxide loaded H-Beta

Catalysts	B27	5GaB27	B37	5GaB37	B300	5Ga B300
Strong Bronsted Acid (μmol/g of catalyst)	2368	733.9	698.8	448.1	112.9	84.17

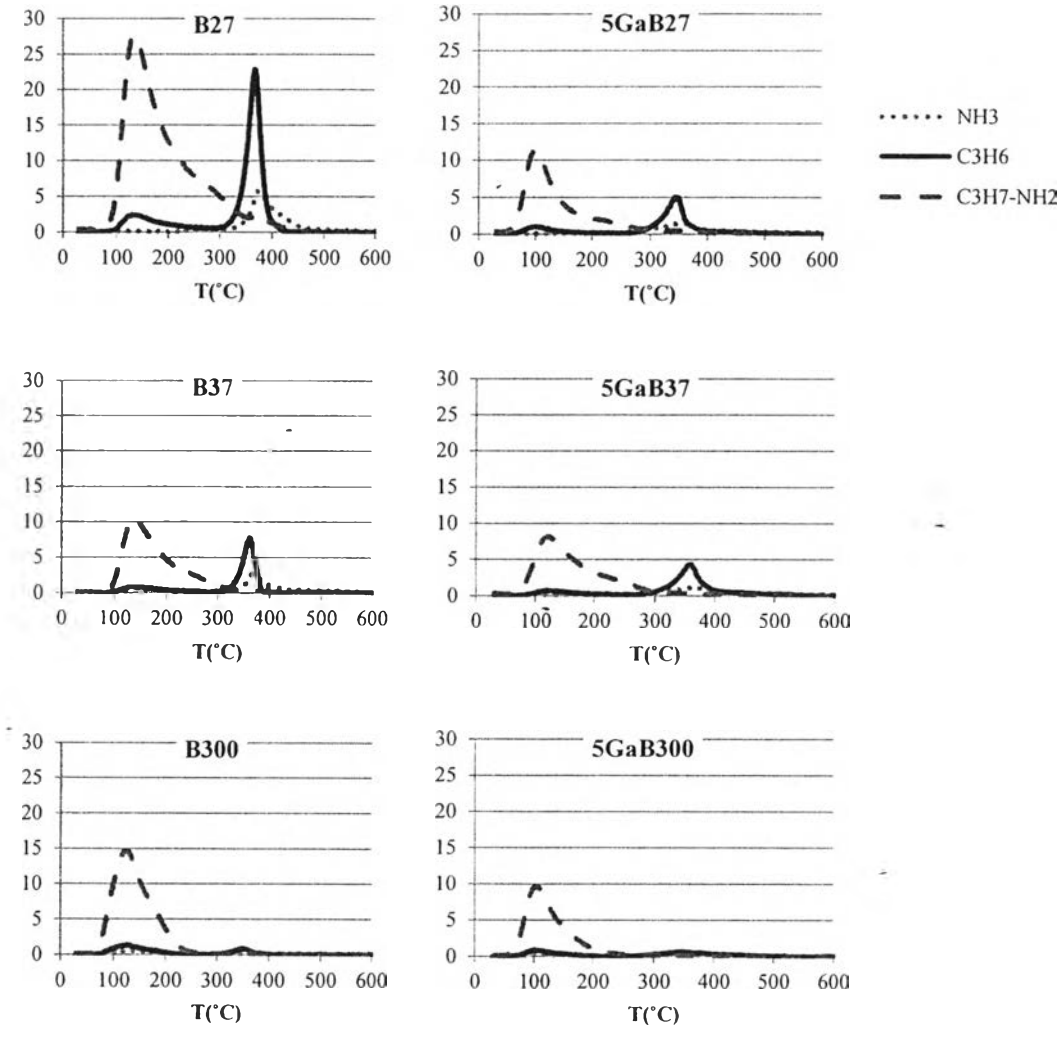

Figure 4.13 TPD-IPA profiles of H-Beta and gallium oxide-modified H-Beta catalysts with different Si/Al_2 ratio.

4.2.2 Activity on Catalytic Dehydration of Bio-ethanol

More than 97% ethanol conversion is achieved over all Si/Al_2 ratio of modified H-Beta. Ethylene is first produced from ethanol dehydration, and then ethylene is converted into various hydrocarbon products, which is governed by acidity or Si/Al_2 of H-Beta zeolite. From Table 4.8, all modified H-Beta catalysts produce gas as the main product. Only 6.48 % oil is obtained from 5GaB37, that is the highest among those obtained from the other gallium oxide modified catalysts.

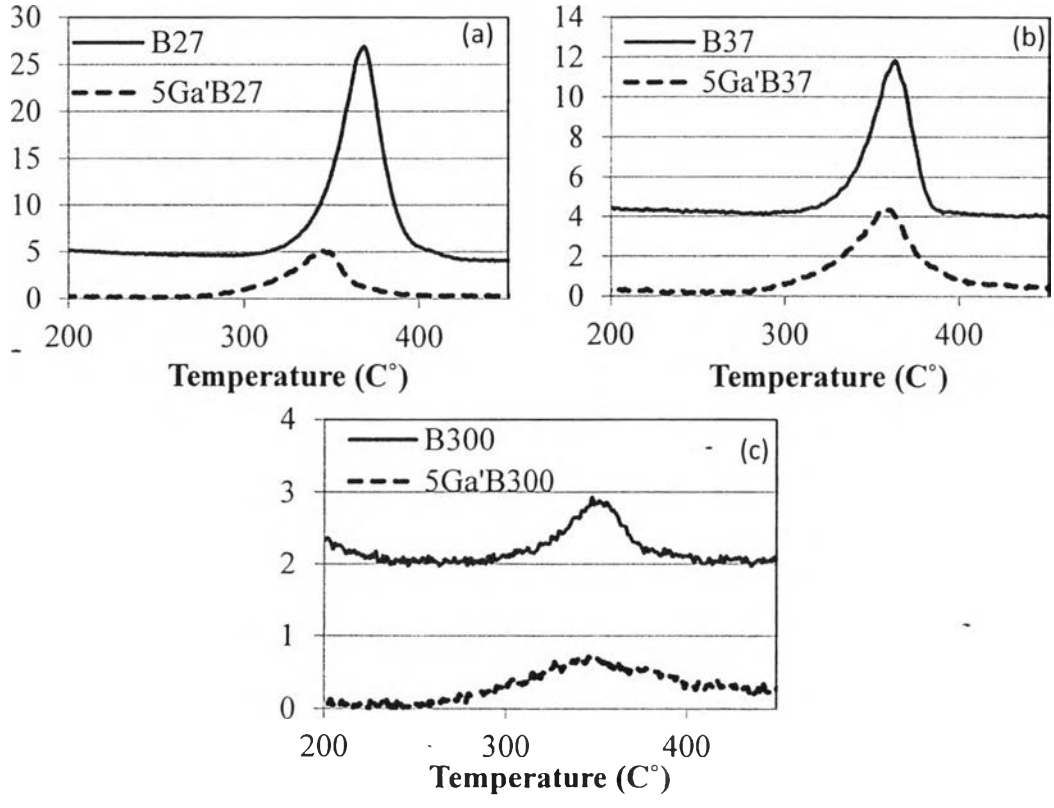

Figure 4.14 Propylene desorption profiles of 5% wt gallium oxide-loaded H-Beta catalysts (a) 5GaB27, (b) 5GaB37, and (c) 5GaB300 from TPD-IPA.

For the gas composition, the major gaseous component in all catalysts is ethylene, which is 73.8 % to 95.5 % in the gas product. 5GaB37 gives a noticeable larger gas composition; that is, 13.4 % C3 and 5.40 % C4. The lower acid density of 5GaB300 produces ethylene mainly. So, the moderate acid density and acid strength of 5GaB37 prefers to convert ethylene to large hydrocarbons in gas.

For the oil phase, 3.11 to 6.48 % of oil is attained from secondary reactions in the reaction pathway (Inaba *et al.*, 2006). 5GaB27 produces the oil that consists of 66.5 % BTEX, 26.9 % C_9 aromatics, and a little amount of other hydrocarbons products as shown in Figure 4.16 (a). However, the oil composition from 5GaB37 shows that 15.6 % C_9 aromatics, 39.0 % C_{10}^+ aromatics, and 18.8 % non-aromatics are mainly produced, but BTX are produced in a low amount.

Table 4.8 Product distribution over all Ga_2O_3–modified catalysts

Catalyst	B 27	5Ga B27	B 37	5Ga B37	B 300	5Ga B300
Bio-ethanol conversion	97.4	97.4	97.4	97.4	97.4	97.4
Product distribution (wt %)						
Gas	75.8	83.7	63.0	75.4	81.5	78.6
Oil	5.05	3.92	7.27	6.48	5.43	3.11
Water	19.2	12.4	29.7	18.1	13.1	18.3
Gas composition (wt %)						
Methane	0.99	1.34	1.65	1.28	0.00	0.00
Ethylene	85.9	87.1	80.4	73.8	94.6	95.5
Ethane	5.61	5.27	6.29	6.16	1.69	1.53
C3	5.85	5.10	8.88	13.4	2.82	2.27
C4	1.66	1.22	2.80	5.40	0.91	0.41
CO_2	0.00	0.00	0.00	0.00	0.00	0.99

Data were taken at the eighth hour of time-on-stream

The acid density and acid strength of 5GaB27 and 5GaB37 are compared in Figure 4.12. 5GaB27 has lower acid density, but higher acid strength, whereas 5GaB37 has higher acid density, but lower acid strength. So, the protons on 5GaB27 can more easily protonate small hydrocarbons to short chain aromatics than those on 5GaB37; however, a less acid density on 5GaB27 does not allow long-chain aromatic hydrocarbons to grow as much as on 5GaB37 that has a higher acid density. That is the reason why 5GaB27 produces more BTX, less oil yield, and less long-chain aromatics (C_9^+). For 5GaB37, the larger amount of weaker acid sites protonates ethylene, and allows longer chain hydrocarbons to grow. It can be explained that ethylene, which is the major component in the gaseous phase, can be further converted to benzene via oligomerization and aromatization reactions. After that, the

alkylation of benzene with ethylene generates ethylbenzene. A large amount of benzene, C_9- and C_{10}^+ aromatics are formed from dispropotionation and transalkylation reactions. On the other hand, 5GaB300, which has the lowest acid density and acid strength, produces 83.7 % gas and only 3.11 % oil. Moreover, it produces a large amount of 45.1 % oxygenates (cyclopropanenonanoic acid, methyl ester, tridecanoic acid, methyl ester, 2-pentanone, and 10-undecyn-1-ol) and a low amount of hydrocarbons.

The true boiling point curves (TBPs) of the extracted oils are cut based on the boiling point ranges of petroleum fractions. 5GaB37, which produces the highest amount of oil and heavy products, gives 33.1 % kerosene, which is the highest among the other catalysts. The oil from 5GaB27 has a high boiling point in gas oil range because the catalyst has the highest acid strength. 5GaB300 produces 84.4 % gasoline that is the fraction containing BTEX and oxygenate compounds.

4.3 Effect of Germanium Oxides Loaded on Beta Zeolites

4.3.1 Characterization of Catalysts

For XRD results, the specific peaks of germanium oxide are shown at 52.2 ° and 61.6 °. However, the specific peaks of H-Beta zeolite are still present in the XRD pattern after loading with both metal oxides, meaning that the germanium oxide loading does not affect the zeolite structures.

Germanium oxide further reduces the surface area and pore volume from those of unloaded zeolites because of pore blocking from metal oxide; for example, the surface area of B37 reduces from 502.7 m^2/g to 432.2 m^2/g after germanium oxide loading, and the pore volume of modified catalysts decreases with the same trend.

For TPD-IPA, Figure 4.20 indicates obviously decreasing acid density and acid strength of catalysts after germanium oxide loading, except 5GeB300. Additionally, germanium oxide tends to significantly reduce the acid strength of catalysts as shown in Figure 4.21.

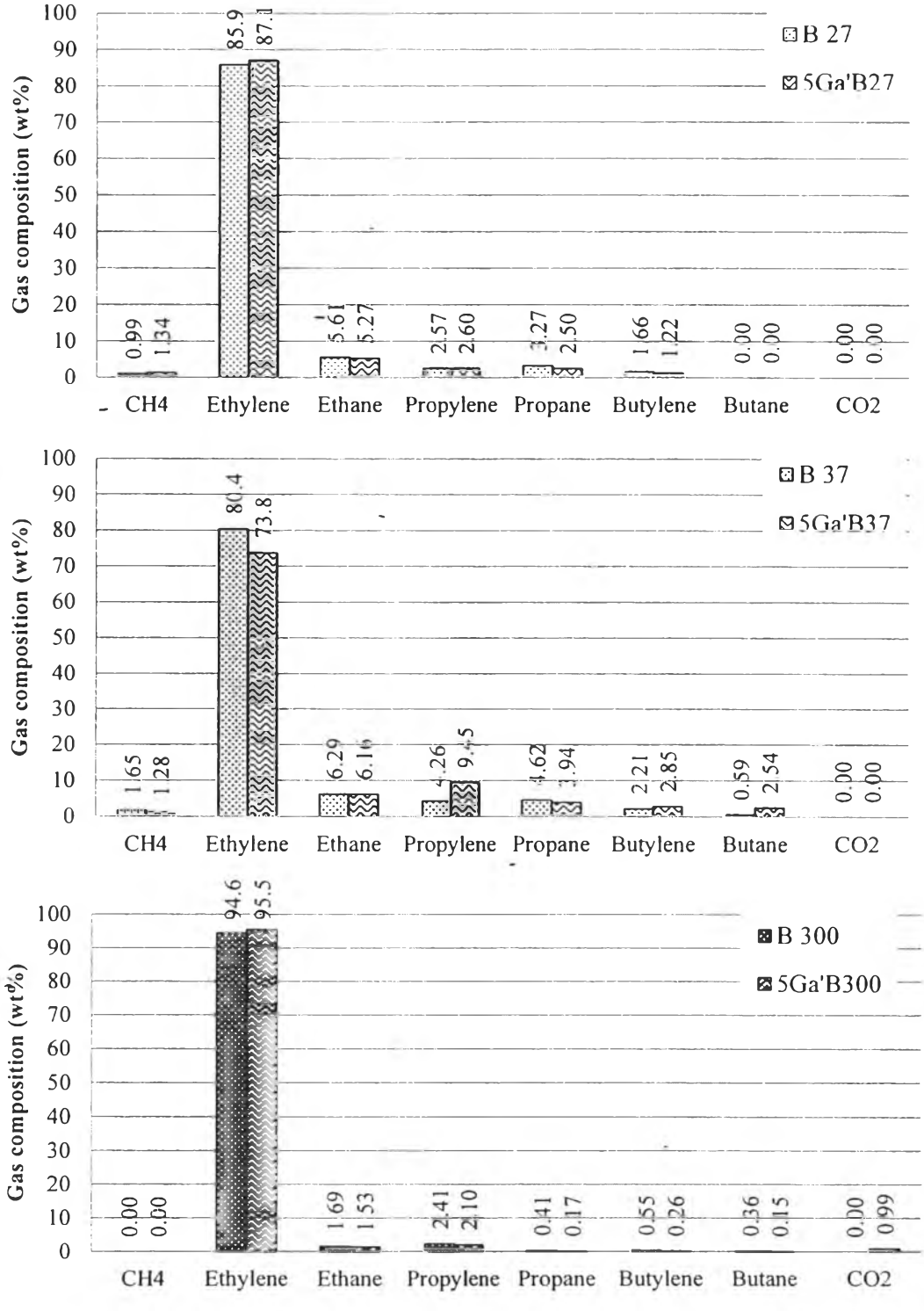

Figure 4.15 Composition of gaseous products from using Ga_2O_3-modified catalysts.

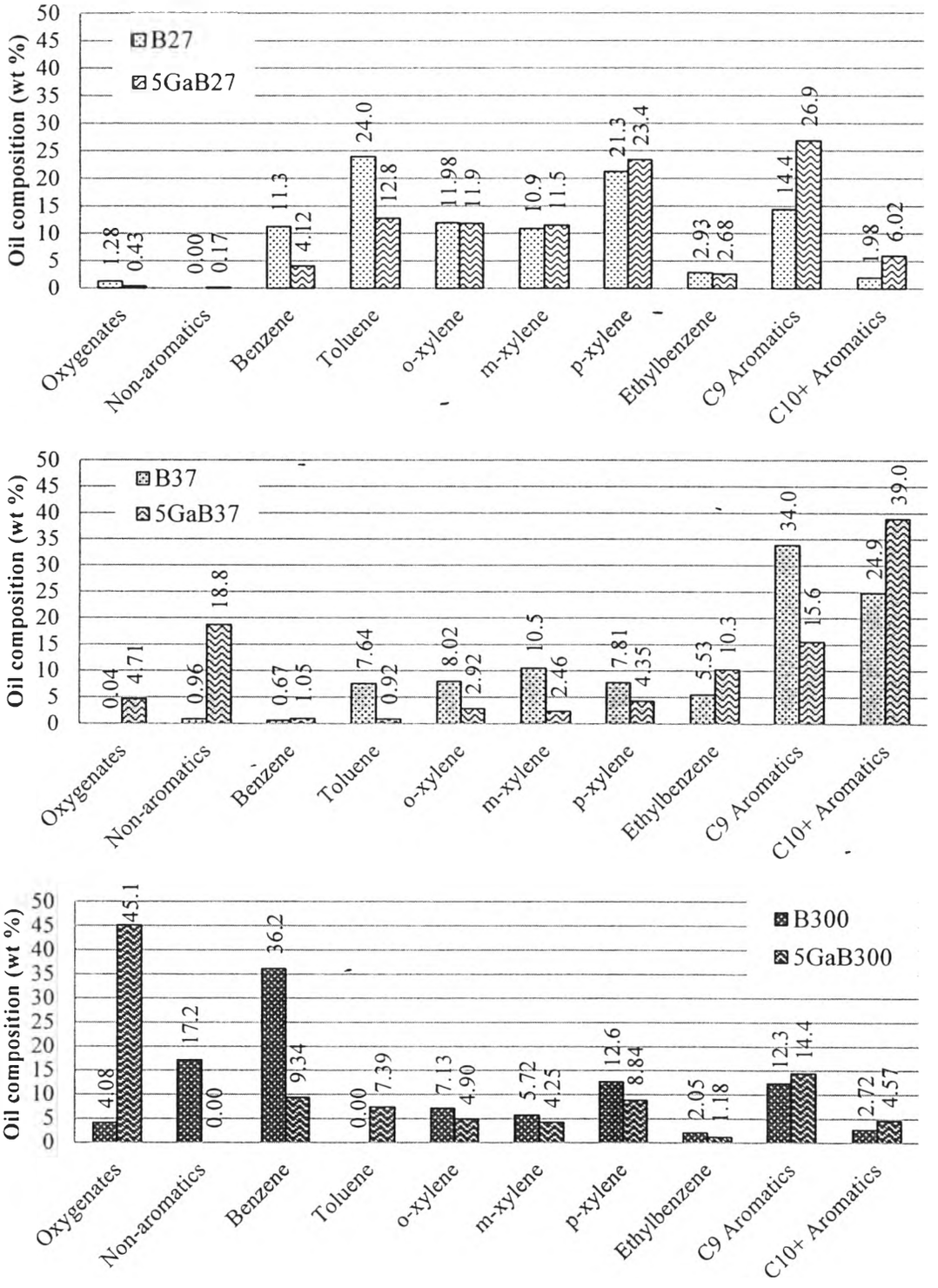

Figure 4.16 Composition of extracted oils from using Ga_2O_3-modified catalysts.

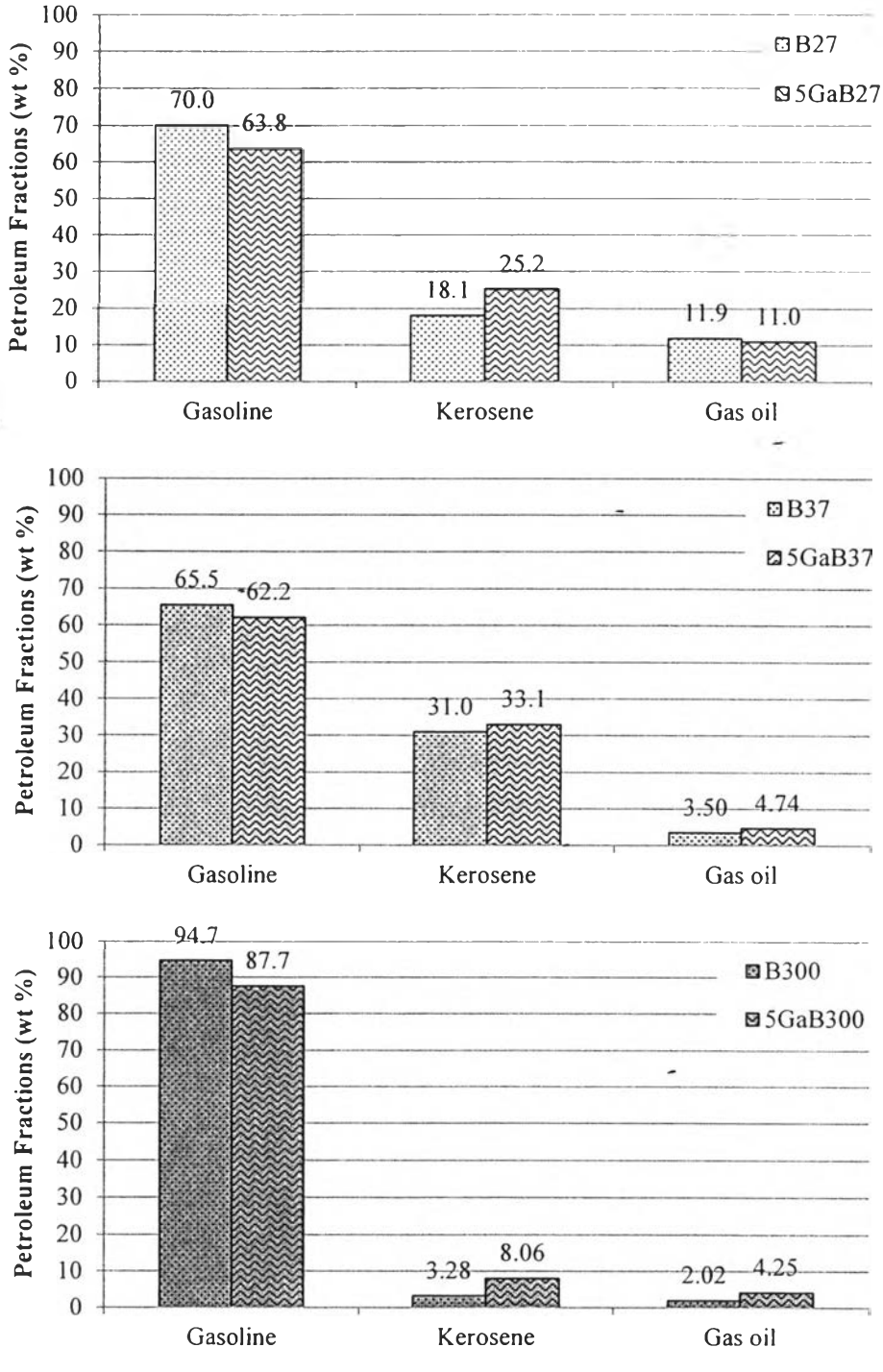

Figure 4.17 Petroleum fractions in oils derived from using Ga_2O_3-modified catalysts.

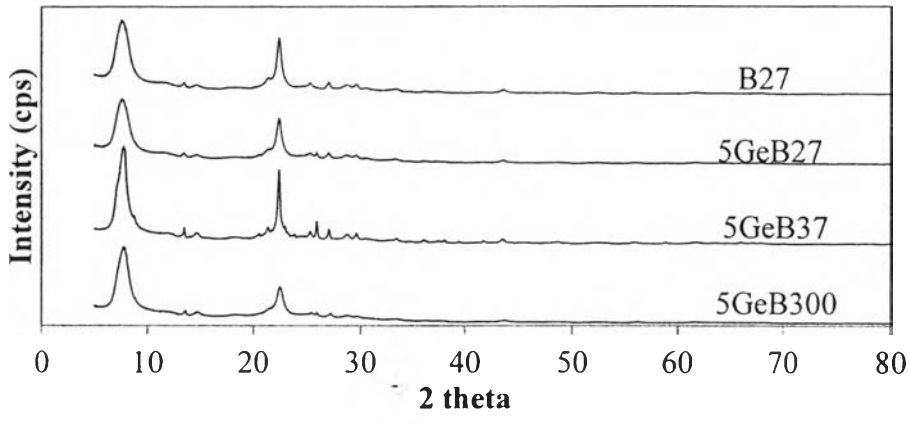

Figure 4.18 XRD characteristic peaks of H-Beta.

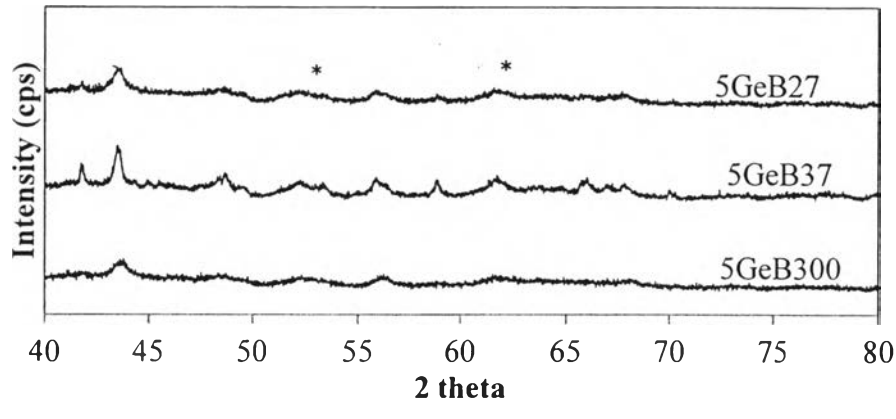

Figure 4.19 XRD characteristic peaks of germanium oxide-loaded H-Beta catalysts.

Table 4.9 Physical properties of germanium oxide-loaded catalysts

Catalysts	B27	5GeB27	B37	5GeB37	B300	5GeB300
Surface Area[a] (m^2/g)	554.9	494.7	502.7	432.2	425.9	395.0
Pore Volume[b] (cm^2/g)	0.27	0.24	0.26	0.22	0.20	0.19
Pore Diameter[b] (Å)	7.68	8.11	7.93	7.82	8.67	7.36

[a] Determined by BET method
[b] Determined by H.K. method

Table 4.10 Density of Bronsted acid site over unloaded H-Beta and 5 wt % germanium oxide loaded H-Beta

Catalysts	B27	5Ge B27	B37	5Ge B37	B300	5Ge B300
Strong Bronsted Acid (μmol/g of catalyst)	2367.5	616.9	698.8	639.3	112.9	119.6

4.3.2 Activity on Catalytic Dehydration of Bio-ethanol

Bio-ethanol conversion using unmodified zeolites and GeO_2 modified zeolites is around 97 %. It indicates that GeO_2 modification does not significantly affect the bio-ethanol conversion. The products from GeO_2-modified zeolites contain approximately 70 % to 80 % gas and 5% oil as shown in Table 4.11. Figure 4.22 illustrates that ethylene is a main gas component in all catalysts, and its amount depresses when GeO_2 is used to modify B27 and B300. However, 5GeB37 shows the opposite trend from 5GeB27 and 5GeB300. Moreover, the other gaseous products are produced at an insignificantly different low amount. However, 5 % GeO_2 loaded on H-beta zeolites gives the product distribution in the extracted oils as shown in Figure 4.23. On B27 and B37, GeO_2 tends to produce lower BTX components in oils; however, C_{10}^+ aromatics are increased. In addition, C_{10}^+ aromatics selectivity is enhanced to 41.0 % using germanium oxide-modified B37. 5GeB300 exhibits the product distribution in the extracted oil in a dissimilar trend; that is, benzene, C_9- and C_{10}^+ aromatics decrease, but oxygenate compounds is extremely enhanced.

Figure 4.24 shows that the true boiling point curves (TBPs) of extracted oils are cut based on the boiling point ranges of petroleum fractions. All catalysts mainly produce more than 60 % gasoline, but only B 300 produces as high as around 80 % gasoline. Figure 4.24 displays the reduction of gasoline and the increases in kerosene and gas oil with germanium oxide loading. These results indicate that germanium oxide may assist to improve the acidity of H-beta zeolites. Additionally, it can be concluded that germanium oxide modification enhances the production of heavy hydrocarbons in the ranges of kerosene and gas oil.

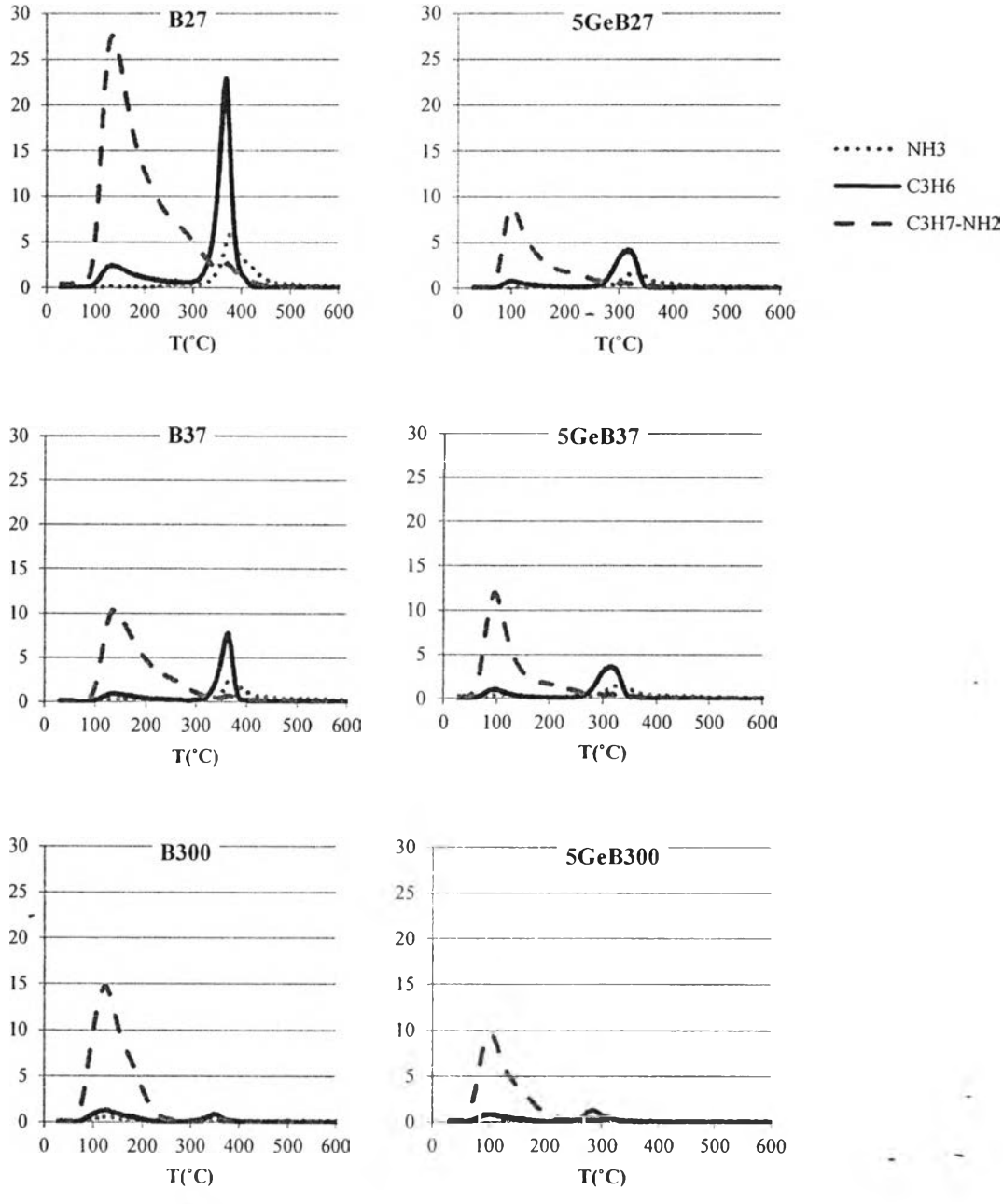

Figure 4.20 TPD-IPA profiles of H-Beta and germanium oxide-modified H-Beta zeolites with different Si/Al_2 ratio.

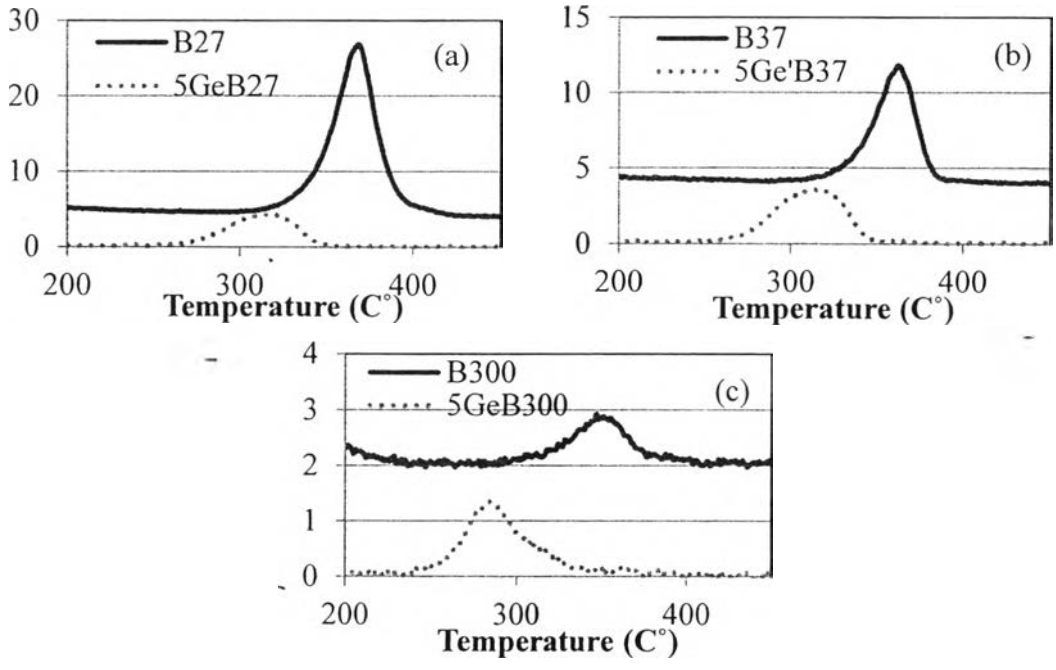

Figure 4.21 Propylene desorption profiles of 5% wt germanium oxide-loaded H-Beta catalysts (a) 5GeB27, (b) 5GeB37, and (c) 5GeB300 from TPD-IPA.

Table 4.11 Product distribution over all GeO_2–modified catalysts

Catalyst	B 27	5Ge B27	B 37	5Ge B37	B 300	5Ge B 300
Bio-ethanol conversion (%)	97.4	97.4	97.4	97.4	97.4	97.4
Product distribution (wt %)						
Gas	75.8	80.0	63.0	68.5	81.5	70.2
Oil	5.05	5.04	7.27	4.62	5.43	4.81
Water	19.2	14.1	29.7	26.8	13.1	25.0
Gas composition (wt %)						
Methane	0.99	5.57	1.65	1.44	0.00	0.16
Ethylene	85.9	77.4	80.4	85.7	94.6	81.7
Ethane	5.61	7.16	6.29	4.62	1.69	1.43
C3	5.85	7.72	8.88	6.70	2.82	2.68
C4	1.66	2.19	2.80	2.55	0.91	1.27
CO_2	0.00	0.00	0.00	0.00	0.00	0.30

Data were taken at the eighth hour of time-on-stream

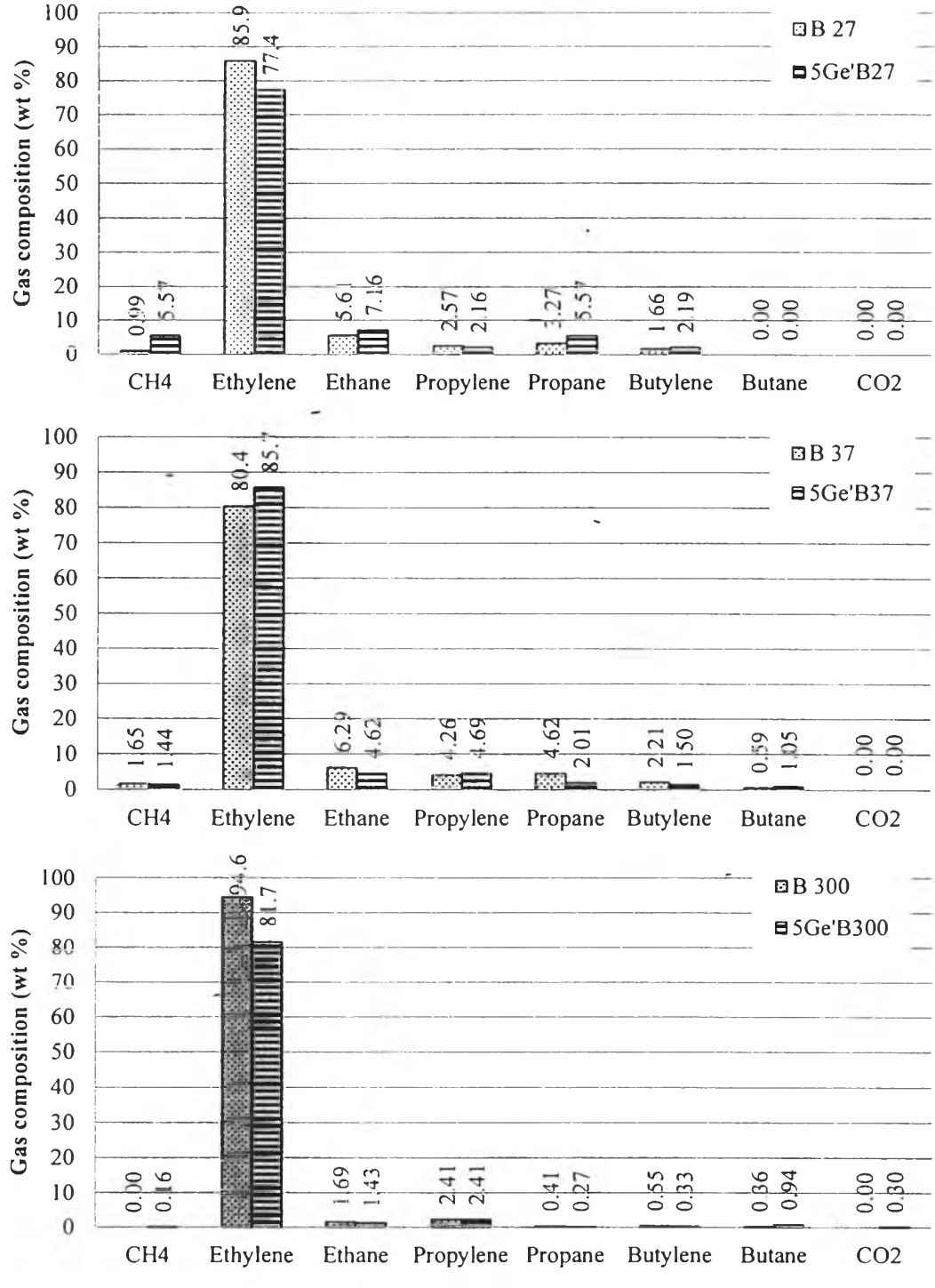

Figure 4.22 Composition of gaseous products from using GeO_2-modified catalysts.

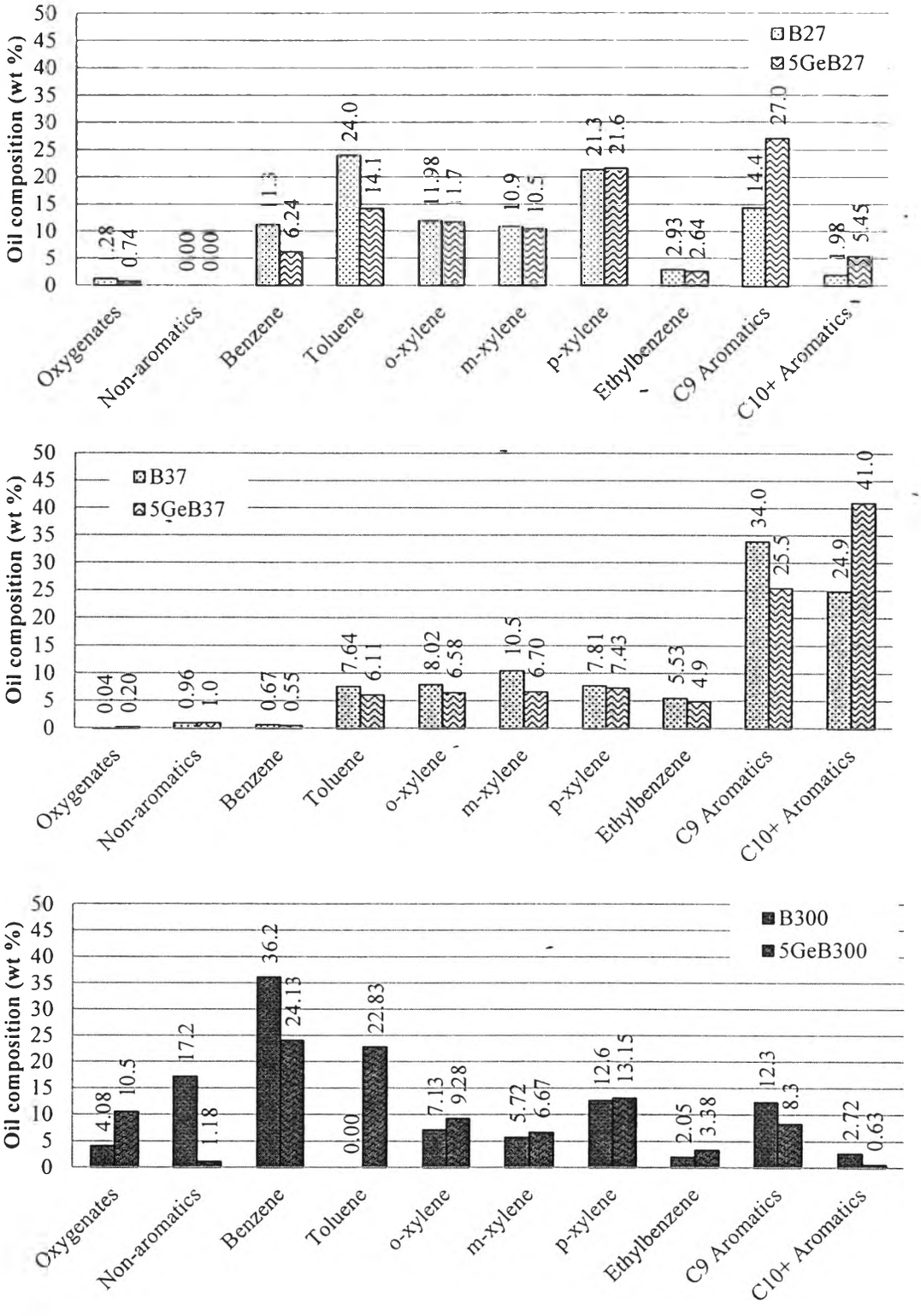

Figure 4.23 Composition of extracted oils from using GeO_2-modified catalysts.

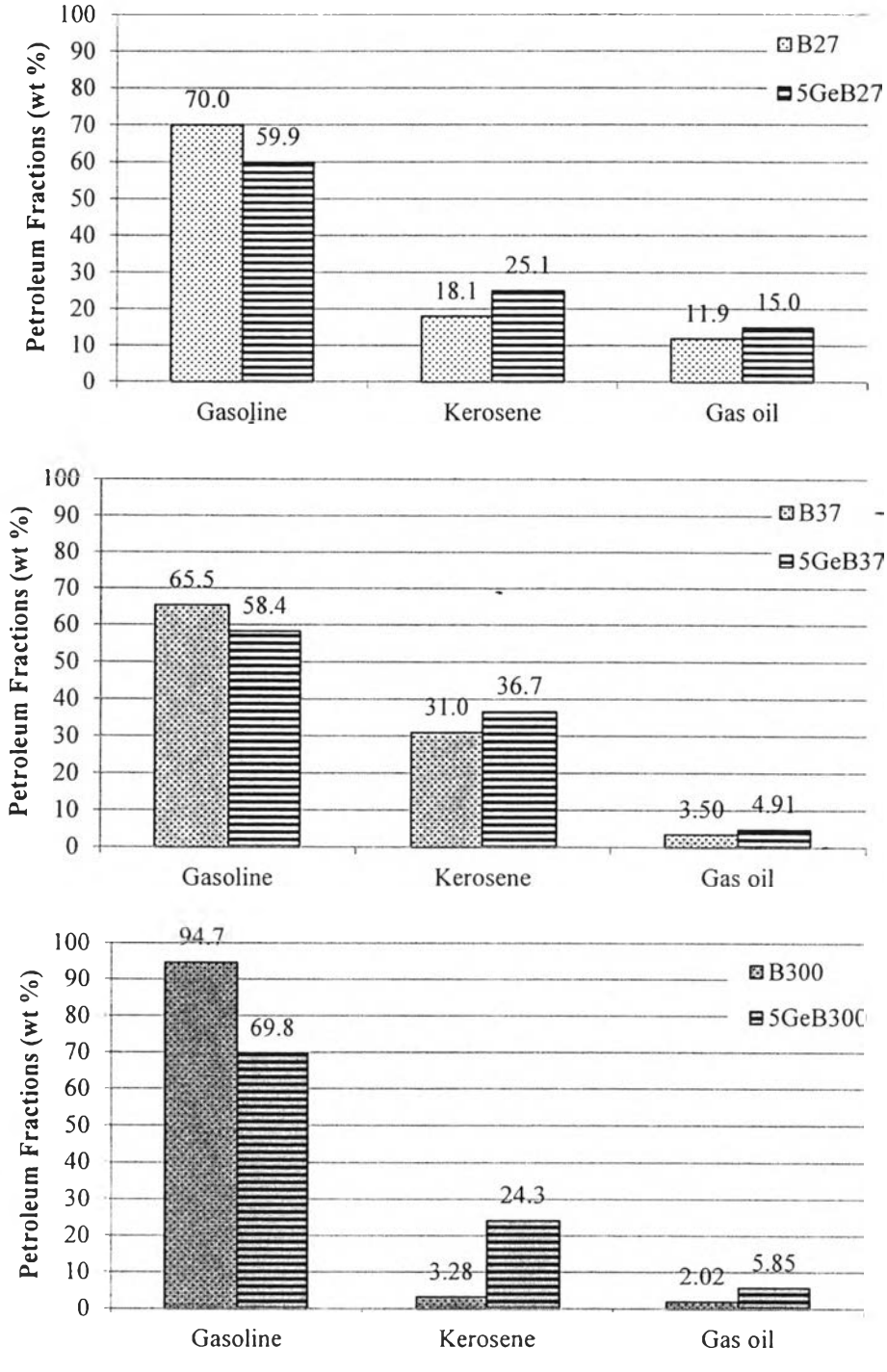

Figure 4.24 Petroleum fractions in oils derived from using GeO_2-modified catalysts.

4.4 Activity of Mesoporous Catalyst (MSU-S, Hexagonal Pore Structure) on Catalytic Dehydration of Bio-ethanol

The mesoporous catalyst with hexagonal pore structure (MSU) was synthesized, following the procedures in a paper (Triantafyllidis *et al.*, 2007). Thus, this catalyst requires many characterizations to confirm the structure before use in catalytic activity testing. XRD (small angle), XRF, SAA, and TPD-IPA are used for characterizing the catalysts.

4.4.1 Characterization of Catalysts

The small angle XRD pattern of MSU is presented in Figure 4.25 (a). MSU displays a strong peak of [100] and the two other peaks that clearly indicate the highly ordered hexagonal pore structure (Liu *et al.*, 2001). Figure 4.25 (b) displays the wide angle XRD pattern of MSU that indicates its non-crystalline structure.

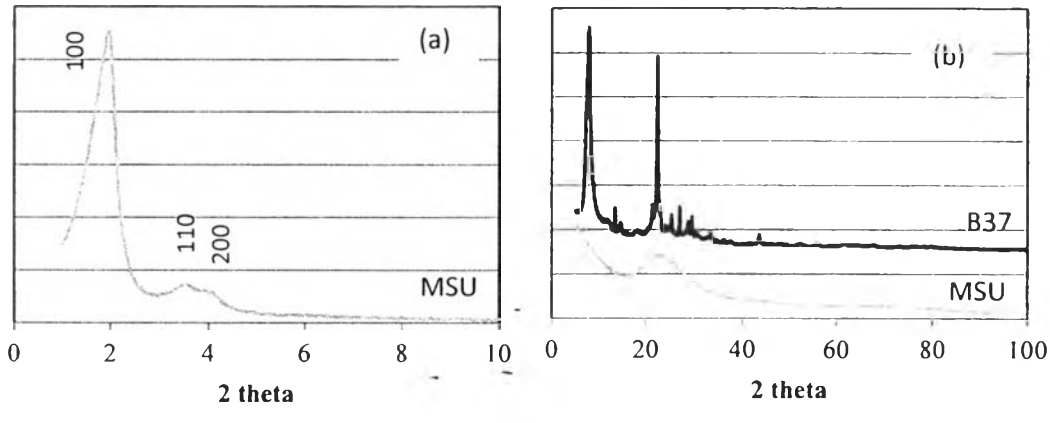

Figure 4.25 X-ray diffraction patterns of (a) MSU at small angles, and (b) H-Beta and MSU at wide angles.

A Si/Al_2 ratio of MSU is 81.1, which was characterized using XRF. A large amount of silica is present in MSU to maintain a mesoporous structure.

The SAA provides the N_2 adsorption-desorption isotherm, pore diameter (micro- and meso pore), pore size distribution, surface area, and pore

volume. In Figure 4.26, the N_2 adsorption-desorption isotherm presents sudden step at the P/P_0 of around 0.3, which is very similar to that of classical hexagonal Al-MCM-41 (Triantafyllidis *et al.*, 2007). Porous MSU contains micro- and meso pores, whose sizes can be calculated by using H.K. and B.J.H. method, respectively as shown in Table 4.12. Figure 4.27 shows that the maximum meso pore size is nearby 30 Å, which is similar to the pore size reported in the literature.

For modified MSU catalysts, the XRD pattern and adsorption-desorption isotherm are same as that of MSU. From Table 4.12, the surface area and pore volume of modified MSU catalysts are enhanced; on the other hand, the meso pore diameter decreases because those metal oxides may be deposited in the meso pore of catalysts.

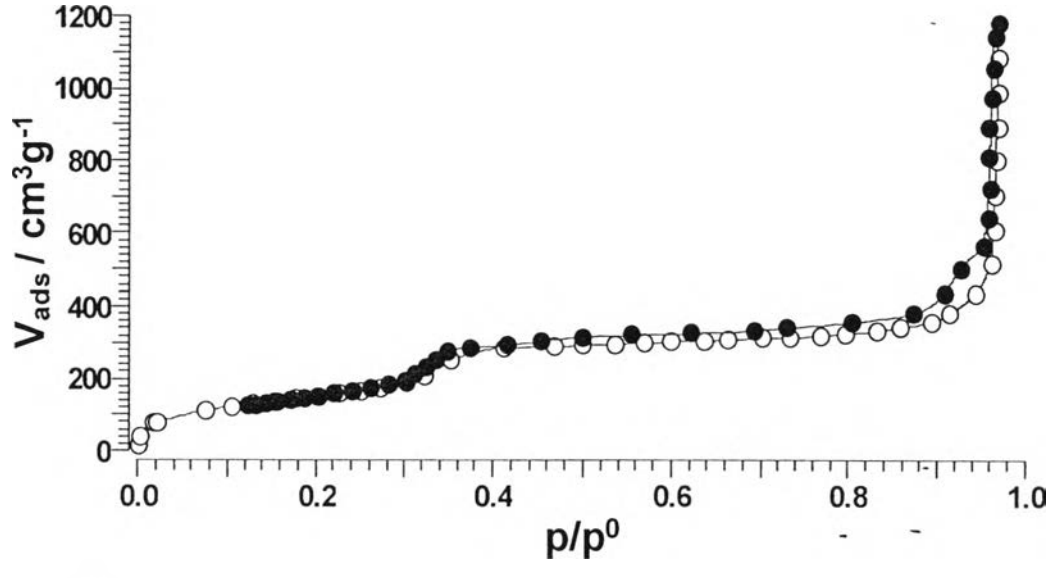

Figure 4.26 N_2 adsorption-desorption isotherm of the MSU catalyst.

The IPA-TPD of any MSU catalyst illustrates a large area of IPA desorption that represents a high Lewis acid density of the extra-framework aluminum, whereas the propylene desorption is present in a small amount. Gallium oxide loading significantly decreases Lewis and Bronsted acid densities as shown in

Figure 4.28. On the other hand, Figure 4.29 presents obviously diverse acid stranght of MSU and germanium oxide-loaded MSU catalyst.

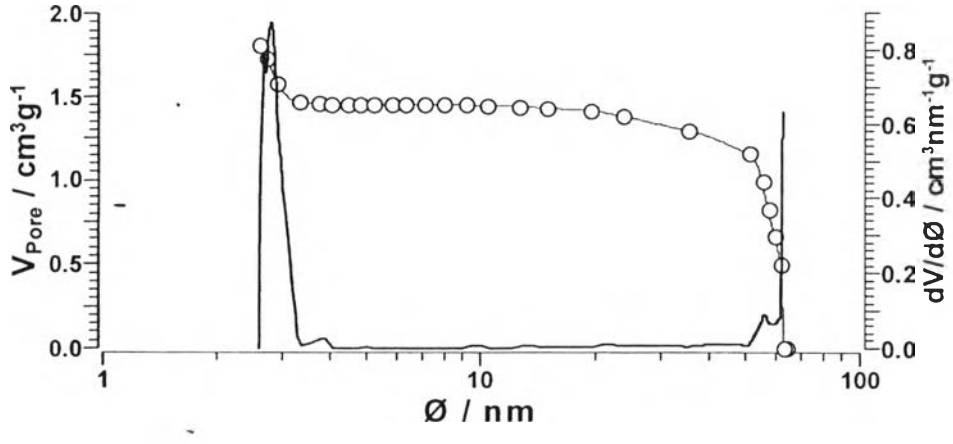

Figure 4.27 Pore size distribution of MSU using B.J.H. method.

Table 4.12 Physical properties of MSU and modified MSU catalyst

Catalysts	Surface Area (m^2/g) [a]	Pore Volume (cm^3/g) [b]	Micro-Pore Diameter (Å) [b]	Meso-Pore Diameter (Å) [c]
MSU	579.9	0.23	10.4	27.6
5GaMSU	652.1	0.28	9.41	26.9
5GeMSU	664.7	0.29	9.44	26.9

[a] Determined by BET method
[b] Determined by H.K. method
[c] Determined by B.J.H. method

4.4.2 Bio-ethanol Dehydration Activity

The product distribution of MSU is not strongly different from that of H-Beta zeolites, which gives 4.47 % oil. 93.6 % ethylene is the highest content in the gas product. Moreover, all modified MSU catalysts give insignificantly different gas compositions as shown in Table 4.14.

A large amount of xylenes, C_9- and C_{10}^+ aromatics are formed using MSU mesoporous catalysts because the large meso pore size improves the diffusion

of large hydrocarbons. From Figure 4.30, the germanium oxide-modified MSU catalyst has similar products that are produced by using MSU catalyst, except C_{10}^{+} that is significantly enhanced. On the other side, the distribution of compounds in oil from gallium oxide-loaded MSU is markedly changed; that is, 92.4 % oxygenates (87.5 % 2-butanone) are produced.

For the petroleum fractions as shown in Figure 4.31, MSU and 5GeMSU catalysts can produce a higher amount of kerosene than H-Beta catalysts because of the mesopore. However, almost the oil components from 5GaMSU, which have oxygenates as a main product, are in the gasoline range.

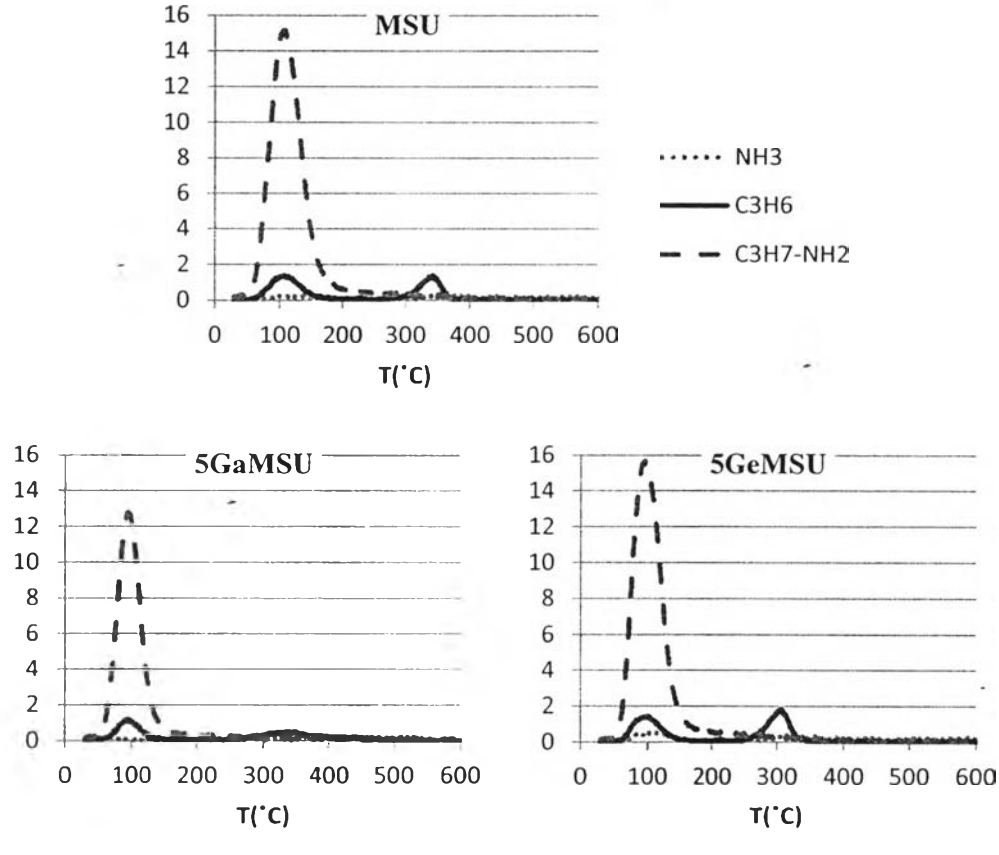

Figure 4.28 TPD-IPA profiles of MSU and modified MSU catalysts.

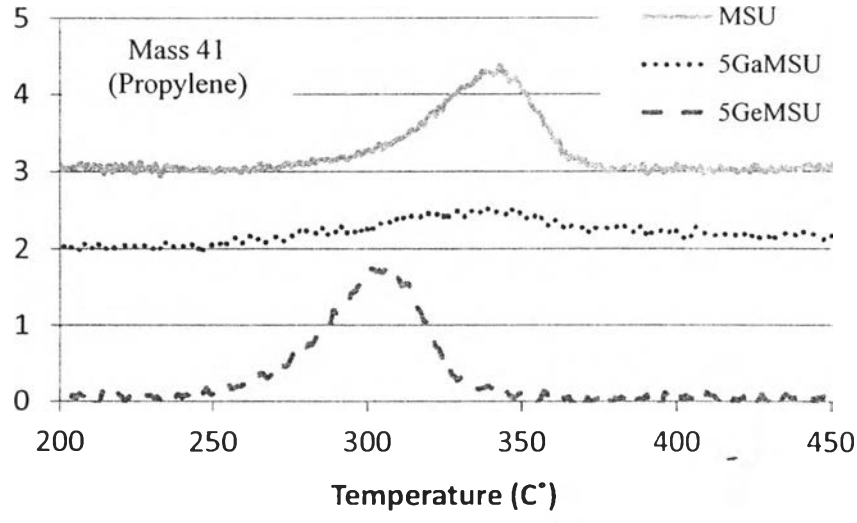

Figure 4.29 Propylene desorption profiles of MSU and modified MSU catalysts from a TPD-IPA technique.

Table 4.13 Density of Bronsted acid sites over MSU and modified MSU catalysts

Catalysts	MSU	5GaMSU	5GeMSU
Strong Bronsted Acid (μmol/g of catalyst)	177.5	49.44	155.0

Table 4.14 Product distribution over Ga_2O_3–and GeO_2-modified MSU catalysts

Catalyst	MSU	5GaMSU	5GeMSU
Bio-ethanol Conversion (%)	97.3	97.3	97.3
Product Distribution (wt %)			
Gas	77.4	79.6	75.3
Oil	4.47	5.17	6.95
Water	18.2	15.2	17.7
Gas Composition (wt %)			
Methane	0.44	0.65	0.25
Ethylene	93.6	92.8	94.4
Ethane	1.38	1.36	1.52
C3	2.66	2.23	1.91
C4	1.71	1.67	1.62
CO_2	0.17	1.26	0.29

Data were taken at the eighth hour of time-on-stream

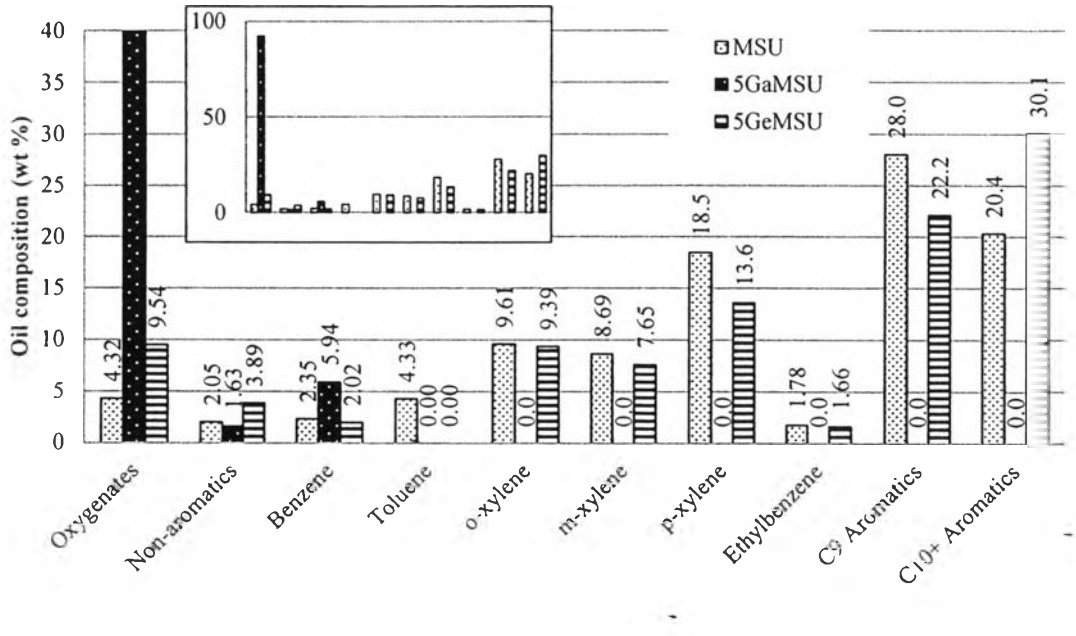

Figure 4.30 Composition of extracted oils from using MSU and MSU-modified catalysts.

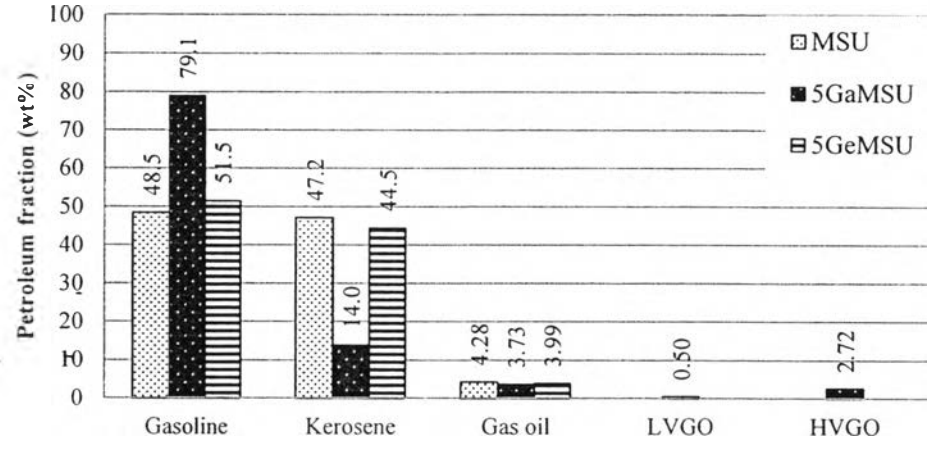

Figure 4.31 Petroleum fractions in oils derived from using MSU and-modified catalysts.